Structural basis for coupling of the WASH subunit FAM21 with the endosomal SNX27-Retromer complex

Qian Guo[1,†], Kai-en Chen[1,†], Manuel Gimenez-Andres[2,†], Adam P. Jellett[2], Ya Gao[1], Boris Simonetti[2], Meihan Liu[1], Chris M. Danson[2], Kate J. Heesom[3], Peter J. Cullen[2,‡], Brett M. Collins[1,‡].

[1] The University of Queensland, Institute for Molecular Bioscience, St Lucia, Queensland, 4072, Australia.

[2] School of Biochemistry, Faculty of Life Sciences, Biomedical Sciences Building, University of Bristol, Bristol BS8 1TD, UK.

[3] Bristol Proteomics Facility, School of Biochemistry, Faculty of Life Sciences, Biomedical Sciences Building, University of Bristol, Bristol BS8 1TD, UK.

[†]Contributed equally

[‡]Corresponding author: pete.cullen@bristol.ac.uk; b.collins@imb.uq.edu.au

Running title: SNX27-Retromer interaction with WASH.

Key Words: Retromer, SNX27, endosome, WASH, AlphaFold, FAM21.

ABSTRACT

Endosomal membrane trafficking is mediated by specific protein coats and formation of actin-rich membrane domains. The Retromer complex coordinates with sorting nexin (SNX) cargo adaptors including SNX27, and the SNX27–Retromer assembly interacts with the WASH complex which nucleates actin filaments establishing the endosomal reycling domain. Crystal structures, modelling, biochemical and cellular validation reveal how the FAM21 subunit of WASH interacts with both Retromer and SNX27. FAM21 binds the FERM domain of SNX27 using acidic-Asp-Leu-Phe (aDLF) motifs similar to those found in the SNX1 and SNX2 subunits of the ESCPE-1 complex. Overlapping FAM21 repeats and a specific Pro-Leu containing motif bind three distinct sites on Retromer involving both the VPS35 and VPS29 subunits. Mutation of the major VPS35-binding site does not prevent cargo recycling, however it partially reduces endosomal WASH association indicating that a network of redundant interactions promote endosomal activity of the WASH complex. These studies establish the molecular basis for how SNX27–Retromer is coupled to the WASH complex via overlapping and multiplexed motif-based interactions required for the dynamic assembly of endosomal membrane recycling domains.

Significance Statement

Cell surface transmembrane proteins are regulated by a constant cycle of internalization and recycling from intracellular endosomal compartments. The Retromer protein complex and the sorting nexin adaptor protein play a critical role in the retrieval of hundreds of proteins responsible for ion transport, glucose metabolism, neurotransmission, and other cell functions. We have defined the mechanism by which both Retromer and SNX27 engage the actin-nucleating complex called WASH through multiple repeated sequences in the subunit FAM21. Dysfunction in WASH, Retromer and SNX27 are implicated in various disorders including Parkinson's disease, Alzheimer's disease, hereditary spastic paraplegia, and this work provides important insights into the assembly of these essential endosomal sorting machineries.

INTRODUCTION

Maintenance of appropriate levels of endosomal sorting of transmembrane 'cargo' proteins is essential for cellular function (1). Mammalian Retromer is an evolutionarily conserved protein complex composed of VPS35, VPS29, and VPS26 (two isoforms VPS26A and VPS26B) and is a central regulator of endosomal sorting across eukaryotes (2, 3). More specifically, it functions together with diverse accessory proteins and cargo adaptors to coordinate endosomal recruitment and sequence-specific cargo recognition with the assembly of endosomal sub-domains for the biogenesis of tubulovesicular transport carriers. Sorting nexin 27 (SNX27) is a Retromer cargo adaptor that binds to specific PSD95-DLG-ZO1 (PDZ) domain binding motif (PDZbm) containing cargo to promote their Retromer-dependent endosome-to-cell surface recycling (4-8).

Both Retromer and SNX27 associate with the Wiskott-Aldrich Syndrome Protein and SCAR Homolog (WASH) complex, which by driving localised actin polymerisation plays an essential role in endosomal sorting and transport (7-13). The WASH complex is a pentamer of WASHC1, FAM21 (WASHC2), WASHC3 (coiled-coil domain-containing protein 53 (CCDC53)), WASHC4 (KIAA1033; WASH-interacting protein; SWIP) and WASHC5 (Strumpellin; KIAA0196) (9, 10, 14, 15). The WASHC1 subunit is a member of the Wiskott-Aldrich Syndrome Protein (WASP) family (14, 16), and the presence of a C-terminal verprolin homology sequence, connecting sequence, and acidic sequence (VCA) domain allows WASHC1 to activate the actin-related protein 2/3 (ARP2/3) complex to stimulate formation of branched F-actin networks (17). The ARP2/3 complex plays a number of roles in regulating endocytosis and subsequent endosomal sorting and transport processes (18-20).

During endosomal cargo sorting and transport, the WASH complex is essential for the fission of tubules during the biogenesis of transport carriers. Endosomal tubulation is exaggerated in cells lacking the WASH complex (10) and WASH depletion leads to the observation of long endosomal tubules aligned along microtubules (9). It is thought that WASH promotes the scission of cargo-containing tubules via generating F-actin-driven force at the endosomal membrane. Mutations in WASH complex subunits can result in neurological pathologies, such as hereditary spastic paraplegia, inherited intellectual disability, and late-onset Alzheimer's disease (15, 21-24).

Retromer regulates the recruitment of a population of the WASH complex to endosomal membranes (12, 13), while binding of WASHC4 to membrane phosphoinositide lipids can promote Retromer-independent endosomal association. Native immunoprecipitations provided the initital evidence for the WASH complex interacting with Retromer, while yeast two-hybrid assays suggested direct associations between VPS35, FAM21 and WASHC1 (12). Suppression and knock-out of Retromer partly reduces WASH endosomal association (12, 25), while other members of the endosomal protein sorting system are unaffected, such as SNX1 and the RAB5 effector EEA1 (12). Structurally, FAM21 has a 200 amino acid "head" domain that interacts with the WASHC5 and WASHC1 proteins and is crucial for the formation and stabilisation of the WASH complex (13, 14). Following the head domain is a large (around 1100 amino acids) unstructured "tail" domain that contains 21 repeating motifs composed of Leu-Phe and several acidic residues (Asp or Glu) dubbed LFa motifs (26). The enormous unstructured tail of FAM21 is important for membrane association (10), and it was shown that the LFa motifs can bind to the VPS35 subunit of Retromer with the very C-terminal

motifs being most crucial for the interaction (26, 27). Overexpression of the FAM21 tail can displace the WASH complex on the endosome by competing for binding to VPS35 and potentially other effectors (13, 26, 27). Although the VPS35 subunit can associate with the FAM21 tail directly in yeast two-hybrid experiments and in isothermal titration calorimetry (ITC) assays (13, 26), binding is enhanced by other subunits when VPS35 is assembled into the functionally active Retromer complex (27). The interaction of Retromer with WASH via FAM21 is thought to link branched actin polymerisation to cargo protein sorting and trafficking activity, and the long unstructured nature of the FAM21 tail combined with the many LFa repeats likely promotes both avidity for Retromer and flexibility in the relative orientations for dynamic endosomal membrane sorting.

The SNX27 Retromer cargo adaptor was also reported to associate with the WASH complex by coimmunoprecipitation (7). Responsible for recycling over 400 specific transmembrane cargoes from endosomes to the plasma membrane (5, 7, 28-30), SNX27 is a peripheral membrane protein containing, from N-termini to C-termini, PDZ, PX and FERM domains that mediate cargo selection, Retromer recruitment and protein-lipid interactions (4, 30, 31). Notably, SNX27 can bind via its FERM domain to acidic DLF (aDLF) motifs in the N-terminal disordered region of SNX1 and its homologue SNX2 within the BAR domain-containing ESCPE-1 complex (32, 33).

Here we show that the FAM21 subunit of WASH coordinates the interactions with both Retromer and SNX27 via very different mechanisms but incorporating distinct overlapping elements of the repeat sequences in its extended C-terminal domain. Crystal structures, modelling, biochemical and cellular experiments show that the multiple redundant acidic-Asp-Leu-Phe (aDLF) repeat sequences in FAM21 bind to a conserved basic pocket in the SNX27 FERM domains and are essentially identical to the aDLF sequences found in the endosomal proteins SNX1 and SNX2 (32). Overlapping repeated motifs in FAM21 with the consensus sequence [L/I]F[ED]$_{3\text{-}9}$[L/I]F bind two conserved sites towards the C-terminus of Retromer subunit VPS35. These lie opposite to the VSP29 binding site and adjacent to the dimerising surface required for assembling Retromer arches on the membrane. In addition, the last repeat of FAM21 contains a specific Asp-Pro-Leu sequence that binds a third site on VPS29 that is the same region bound by other interactors such as TBC1D5 and ANKRD27. Mutations in these regions perturb FAM21 interaction *in vitro* and in cells, however single mutations in VPS35 are not sufficient to block Retromer-mediated trafficking, consistent with a model whereby the WASH complex engages the endosome and associated proteins through multiple related but redundant motif-mediated interactions.

RESULTS

The FAM21 tail binds to both VPS35 and VPS29 through its repeat sequences

A primary characteristic of FAM21 is the long disordered tail enriched in acidic residues and containing 21 copies of a repeated [I/L]F sequence with C-terminal acidic residues (**Figures 1A and 1B**). This was previously termed the LFa motif and shown to bind directly to the Retromer subunit VPS35 with the final three repeats, 19-21, showing the strongest binding affinity (26). However, suggesting that VPS29 also plays a role in binding FAM21, we recently noted that binding of Retromer and GST-tagged FAM21 composed of repeats 19, 20 and 21 (GST-FAM21$_{R19-R21}$) was slightly reduced in the presence of a macrocyclic peptide that binds via a PL-containing sequence to a conserved site on the VPS29 subunit (34). To examine this, we first tested the binding between Retromer and peptides from human FAM21 repeat 19 (FAM21$_{R19}$), repeat 20 (FAM21$_{R20}$) and repeat 21 (FAM21$_{R21}$). Using ITC, we found FAM21$_{R21}$ alone was able to bind to either Retromer, to the subcomplex composed of VPS29 and VPS35 residues 481 to 796 (VPS29–VPS35$_{481-796}$), as well as VPS29 alone (**Figure 1C; Table S1**). In contrast, FAM21$_{R19}$ and FAM21$_{R20}$ peptides showed a relatively weak Retromer interaction and no interaction at all with VPS29 (**Figure 1C)**. A stronger Retromer interaction was observed when we tested the GST-tagged construct combining repeats 19 and 20 (GST-FAM21$_{R19-R20}$), suggesting some additive effect of these two sequences (**Figure 1D)**. Notably the FAM21$_{R21}$ interaction with VPS29 on its own could be blocked by the addition of inhibitory cyclic peptide RT-D1 (**Figure 1E**) (34), indicating that FAM21$_{R21}$ likely binds to the same conserved VPS29 surface. Unlike other repeats FAM21 repeat 21 also contains a conserved DPL sequence next to the [I/L]Fa motif (**Figure 1B; Figure S1**) and it is this sequence that binds to VPS29 while other repeats bind to VPS35.

Structural basis for the interaction of FAM21 LFa repeats with VPS35

Our data suggests that FAM21 LFa repeats 19 and 20 interact with VPS35 while the divergent DPL-containing repeat 21 can bind VPS29. To understand the molecular basis of how the LFa repeating units bind to Retromer, we attempted to co-crystallize the VPS29–VPS35$_{481-796}$ subcomplex with FAM21$_{R19}$ and FAM21$_{R20}$ peptides. The structure of VPS29–VPS35$_{481-796}$ in complex with FAM21$_{R20}$ peptide was successfully solved at 3 Å resolution with two VPS29–VPS35$_{481-796}$ molecules in the asymmetric unit (**Figure 2A; Table S2**). Although the structure was solved at relatively low resolution, we could observe additional electron density on the surface of VPS35 representing the FAM21$_{R20}$ peptide (**Figure 2B**). The electron density for the FAM21$_{R20}$ peptide is located on a conserved positively charged groove of VPS35 between helices 23 and 25 surrounded by K552, K555, K556 and K559 (**Figures 2B and 2C**). To aid in assigning the FAM21$_{R20}$ residues to the structure as well as investigate the potential binding surface of repeat 19, we used AlphaFold2 modelling to predict complexes of different variations of FAM21 sequences bound to Retromer. These predictions consistently identified two separate binding sites on VPS35 for the FAM21$_{R19-R20}$ LFa repeats (**Figures 2D and 2E**). Inspecting these models closely, we found that repeats 19 and 20 are predicted to bind two distinct positively charged grooves at the C-terminal end of the VPS35 surface that we refer to as Site 1 and Site 2 respectively (**Figure 2E**). The X-ray crystallographic difference density for the FAM21$_{R20}$ peptide aligns with Site 2 and matches well to the residues ^{1296}DDIF^{1299} of repeat 20 predicted in the model (**Figure 2F**). In

139 particular I1298 and F1299 are positioned to interact with K555, K556 and K559 of VPS35 (**Figure 2F**). A
140 notable feature of the predicted structure is that in addtion to the ^{1296}DDIF^{1299} residues the repeated element
141 engages VPS35 via an additional IF sequence interspersed with acidic residues ^{1290}IFDDDMDDIF^{1299} (**Figure**
142 **2F**). Similarly the predictions indicate that the second R19 sequence can bind to Site 1 with a similar dual
143 [I/L]F motif with interspersed acidic residues ^{1262}LFDDNIDIF^{1270} recognising a second positively charged
144 groove composed of K701, K705 and K749 (**Figure 2E**). With the combination of predictions and
145 experimental structure we propose that VPS35 possesses two distinct binding sites for low affinity binding of
146 the multiple LFa sequences in FAM21 (**Figure 1B**)(26). These structures indicate the the LFa motif ideally
147 possesses two [I/L]F sequences with an interveining stretch of Asp and Glu side chains [I/L]F[E/D]$_n$[I/L]F.
148 To further validate if both positively charged grooves of VPS35 are responsible for binding to FAM21
149 we performed co-immunoprecipitation with structurally targeted site-directed mutations of VPS35.
150 Importantly, all mutants retained the ability to assemble into the Retromer heterotrimeric complex **(Figure 2G**
151 **and 2H; Figure S2)**. Consistent with our structural data, binding to FAM21 was significantly affected by the
152 multiple mutations around the repeat 20 binding groove including K552, K555, K556 and K559 (**Figure 2G;**
153 **Figure S2**). The strongest defect in FAM21 binding was observed with the triple mutant composed of K555,
154 K556 and K559 (**Figures 2G and 2I; Figure 2G; Figure S2**), the residues known to form contact with the
155 LFa motif in Site 2. In addition, mutations of other positively charged residues surrounding the core [I/L]F
156 dipeptide including K515S also showed significant defects in binding. It is likely that these residues together
157 form a large positively charged patch on VPS35 for the initial recognition of the acidic repeats of FAM21. A
158 similar defect was also observed in the K701E mutant on the second positively charged groove of Site 1
159 (**Figure 2H**). Notably, we also observed a slight defect in FAM21 binding when we used the VPS35 D620N
160 mutant, the mutation known to be involved in the Parkinson diseases (35, 36). The mutation is distal from the
161 FAM21$_{R19}$ and FAM21$_{R20}$ binding sites but lies next to the VPS35-mediated Retromer dimerization interface
162 as seen in the Retromer-SNX3 and Retromer-SNX-BAR tubular coat complexes (37) (**Figure 2J**). It is possible
163 that the slight defect in FAM21 binding is indirectly caused by interference with Retromer dimerization.
164

165 ***Repeat 21 binds to VPS29 through a classic PL motif interaction***

166 To better understand the association of FAM21 repeat 21 with Retromer we next crystallised the VPS29–
167 VPS35$_{481-796}$ complex with the FAM21$_{R21}$ repeat and determined its crystal structure at a modest 3.4 Å
168 resolution. The structure reveals two VPS29–VPS35$_{481-796}$ molecules in the asymmetric unit. Notably, the
169 dimerization interface in this structure differ from that observed in the FAM21$_{R20}$ bound structure (**Figure**
170 **3A**). Despite the low resolution, we could still observe additional electron density around the conserved
171 hydrophobic pocket of VPS29 (**Figure 3A**). To unambiguously assign the key residues involve in the
172 interaction, we then successfully solved the structure of the VPS29–FAM21$_{R21}$ peptide complex at 2.0 Å
173 resolution (**Figure 3B**). The improved density allowed us to build the PL motif and upstream residues.
174 According to the structure, we could unambiguously observe the density up to D1332, suggesting that the
175 signature [I/L]Fa dipeptide located at position 1330 and 1331 was not involved in the binding (**Figure 3C**). In
176 direct contrast to the FAM21$_{R20}$ structure bound with VPS35, the FAM21$_{R21}$ reveals a typical PL motif binding

mode to VPS29 that superposes well with the previous cyclic peptide structures (**Figure 3D**) and other previous complexes with RidL, TBC1D5, VARP and VPS35L (38-42).

Consistent with the two structures and our mutagenesis studies, AlphaFold2 predictions incorporating the FAM21 sequence with all three repeats 19-21 produced a model with the three repeats bound to the three distinct sites; R19 and R20 respectively binding Site 1 and Site 2 on VPS35 and R21 extending around to bind to the conserved VPS29 surface (**Figure 3E-3H**). Both $FAM21_{R20}$ and $FAM21_{R21}$ peptide observed in the crystal structures fit well to the various models generated by Alphafold2 (**Figure 3G**). It seems very likely other LFa repeats would have the capacity to interact with one or both sites in VPS35. Indeed further analysis using Alphafold2 supports the potential of other repeats to bind VPS35 with similar structures (**Figures 3H; Figure S3**), and we find that repeats 5 and 17 (although not repeat 15), show low affinity for Retromer (**Figure 3I**). Projecting these findings onto the VPS35-mediated Retromer dimer observed in cryotomography structures (37), we expect that the LFa repeats such as $FAM21_{R19,}$ $FAM21_{R20}$ and $FAM21_{R21}$ can potentially use at least two distinct binding modes to engage the membrane-associated Retromer complex. With Repeat 21 bound to VPS29 as the reference point, repeats 19 and 20 and other LFa repeats from FAM21 could physically associate with two adjacent Retromer complexes in *trans* (model 1) or with one copy of Retromer in *cis* (model 2) (**Figure 3J**).

Interaction of FAM21 aDLF motifs with the SNX27 FERM domain

In addition to Retromer, SNX27 has also been reported to bind FAM21 to enable proper cargo recycling (7, 43, 44). To confirm this interaction, we first examined the binding using co-immunoprecipitations with various truncation constructs of GFP-FAM21. Robust association was observed between SNX27 and C-terminal region of FAM21(1109-1341) and FAM21(1250-1341) (**Figure 4A**). A shorter construct of FAM21(1300-1341) however, which lacks all LFa repeats apart from repeat 21, was unable to bind. Using ITC, we found that full-length human SNX27 bound to GST-tagged $FAM21_{R19-21}$ with a K_d of ~6 μM (**Figure 4B; Table S3**). A similar binding affinity was also detected when the FERM domain ($SNX27_{FERM}$) was used instead of the full-length SNX27 (**Figure 4B**), suggesting that the interaction primarily occurs through the FERM domain. We also tested the binding of $SNX27_{FL}$ and $SNX27_{FERM}$ with peptides corresponding to individual repeats $FAM21_{R19}$, $FAM21_{R20}$ and $FAM21_{R21}$ (**Figure 4C and D**). The results further reinforced the co-immunoprecipitation experiments showing that both $FAM21_{R19}$ and $FAM21_{R20}$ peptides bind to SNX27 with a K_d of ~7 μM and ~20 μM respectively, while repeat 21 showed no detectable interaction.

We noted that LFa repeats 19 and 20 (but not repeat 21) also contain sequences that resemble the acidic DLF (aDLF) motifs found in SNX1 and SNX2 previously shown to bind to the FERM domain of SNX27 (32). Indeed, mutations in the $FAM21_{R20}$ peptide substituting the DIF sequence with DSS blocked interaction with $SXN27_{FL}$ completely (**Figure 4E**), indicating that the D[L/I]F motif within repeats 19 and 20 play a major role in binding to SNX27. Sequence analysis of all of the 21 repeats within FAM21, showed that 12 of them also included the same sequence pattern with poly-acidic resides in front of a conserved D[L/I]F motif (**Figure 4F**). We proposed that all of these repeats are potentially able to bind SNX27, and using $FAM21_{R5}$, $FAM21_{R8}$, $FAM21_{R15}$ and $FAM21_{R17}$ peptides as examples we found all four showed micromolar binding affinity to

215 hSXN27$_{FERM}$ (**Figures 4G and 4H**). These ITC data together confirmed that the D[L/I]F motif is the main
216 region responsible for binding to the FERM domain of SNX27, while the poly-acidic residues prior to the
217 D[L/I]F motif play a critical role in facilitating the association.

218

219 ***FAM21 and SNX1/SNX2 share the same binding pocket in the SNX27 FERM domain.***

220 To confirm the molecular basis for how FAM21 binds to SNX27, we first applied Alphafold2 to predict models
221 of SNX27$_{FERM}$ in complex with the subset of FAM21 repeats containing the putative aDLF motifs. Consistent
222 with our expectation, all the FAM21 repeats were predicted to bind the same conserved pocket on the F3
223 module of the SNX27 FERM domain (**Figure S4**), also known to bind to the aDLF motifs from SNX1/SNX2
224 (32, 33). To validate the models we then co-crystallized SNX27$_{FERM}$ with several different FAM21 repeat
225 motifs and crystal structures were determined with FAM21$_{R15}$, FAM21$_{R19}$ and FAM21$_{R20}$. All three complexes
226 were solved in the same space group showing a single FERM domain in the asymmetric unit (**Figures 5A-5C;**
227 **Table S4**). The electron density of the aDLF motif region was clearly visible in the highly conserved positively
228 charged pocket of the SNX27 FERM domain (**Figures 5A-5C**). Superimposition of the three structures
229 revealed a high degree of similarity without any major differences (**Figures 5D and 5E**). Our structures also
230 superposed well to the SNX1 peptide bound complex published previously (32, 33) (**Figure 5F**).

231 To confirm the binding mode of SNX27 binding to FAM21 aDLF sequences we tested mutations in
232 key SNX27 residues. SNX27 R437D and R498D mutants failed to interact with FAM21$_{R19}$ peptide by ITC,
233 while K495D, K496D and K501D reduced binding compared to the wild-type SNX27 (**Figure 5G**). The same
234 pattern of binding was observed by co-immunoprecipitation of proteins from HEK293T cells (**Figure 5H**),
235 although interestingly the K495D, K496D and K501D mutants had a greater impact on the ESCPE-1 complex
236 interaction (represented by SNX6 in these experiments) than FAM21 and the WASH complex. This suggests
237 that R437D and R498D play a central role in forming contacts with both FAM21 and SNX1/SNX2-derived
238 aDLF peptides. In particular, R498 is likely to be responsible for electrostatic attraction with the poly-acidic
239 residues in front of the aDLF motifs. Indeed, comparative unbiased proteomic analysis comparing the
240 interactomes of wild-type SNX27 with the R498D mutant of SNX27 confirmed a significant reduction in
241 association of SNX27(R498D) with subunits of both the WASH and ESCPE-1 complexes (**Figure 5I; Figure**
242 **S5A; Table S2**).

243

244 ***VPS35 Sites 1 and 2 enhance WASH endosomal recruitment but are not required for endosome-to-plasma***
245 ***membrane recycling of Retromer-SNX27 cargo proteins.***

246 We and others previously established that mutations in SNX27 that block interactions with aDLF motifs
247 perturb endosomal retrieval and recycling of the SNX27-interacting cargo GLUT1 by the SNX27-Retromer-
248 ESCPE-1 pathway (32, 33). While this phenotype was ascribed to a defect in SNX1 and SNX2-containing
249 ESCPE-1 complex binding to SNX27 during the hand-over of retrieved cargo into newly forming tubular
250 transport carriers (32), our results here indicate that the SNX27(R498D) mutant not only perturbs SNX1/SNX2
251 association but also binding to the WASH complex. Thus the defect in GLUT1 recycling could be attributed
252 to either or both of these interactions, and it is not possible to design highly specific SNX27 mutations to

distinquish them. Similarly, mutation of VPS29 to perturb the binding of FAM21 R21 will also preclude interactions with other essential proteins such as TBC1D5 and VARP (39, 45, 46). In addition, the highly redundant nature of the multiple overlapping LFa/aDLF repeats in FAM21 preclude the design of single point mutations in the FAM21 tail to test the role of specific sequences. Indeed, we found that although deletion of repeats 19-21 (residues 1250-1341) in the tail could reduce both Retromer and SNX27 interactions (**Figure 4A**), individual point mutations in these repeats had no impact on binding (**Figure S5B**) demonstrating that no single sequence is essential to mediate their binding.

To assess whether the interaction of the WASH complex with VPS35 was important for the endosomal activity we first assessed the localisation of FAM21 in VPS35 knock-out HeLa cells followed by rescue experiments with VPS35 mutations in both Site 1 and Site 2 (K555N/K556L/K559Q/K701E; NLQE mutant)(see **Figure 2G and 2H**). VPS35 KO cells show a modest but significant reduction in the colocalisation of FAM21 to SNX1-positive endosomal domains consistent with previous reports (12, 25). Re-expression of VPS35-GFP WT can partially rescue this mislocalistion, however VPS35(NLQE)-GFP is unable to restore FAM21 recruitment levels indicating the VPS35 interaction is important for promoting WASH complex localisation. Concistent with previous findings (47, 48), we did not observe any statistically significant alteration in the co-localization of CI-MPR with TGN46 in VPS35 KO cells, or in wild-type and mutant VPS35(NLQE) rescued cells **(Figure S5C**). We next assessed the importance of VPS35 interactions with FAM21 for receptor recycling. Rescue experiments were performed in both VPS35 knock-out HeLa cells (**Figure 6B and C**), and in H4 cells (**Figure S5D**) with similar results. As expected, in VPS35 KO cells the cell surface levels of SNX27-Retromer cargos including GLUT1 and Kidins220 were reduced. When GFP-VPS35 was re-expressed the cell surface levels of these proteins recovered partially or totally to normal levels. However, the VPS35(NLQE)-GFP mutant was also able to rescue endosomal recycling of these cargos, suggesting that reduced FAM21 binding to VPS35 on its own is not strictly required for the steady-state recycling of SNX27-Retromer-dependent cargos. Previous studies directly targeting FAM21 have shown that its depletion or knock-out leads to cargo sorting defects (43, 46). It is likely our data can be reconciled through the complex multivalent nature of FAM21 association with Retromer, such that although the VPS35 interaction with FAM21 reduces WASH interaction significantly (**Figure 2G and 2H**), and is required for a proportion of WASH recruitment to endosomal retrieval domains, the other minor sites in VPS29 retain an ability to engage FAM21 and may compensate for its loss. Further, FAM21 can interact with SNX27 and other endosomal proteins such as the Commander complex (25, 49), and the population of WASH associated with endosomes in the asbence of Retromer as seen here (**Figure 6A**) and in other studies (50) provide an added level of potential compensation.

DISCUSSION

In this work we have defined the molecular mechanisms underpinning the direct interactions between Retromer, SNX27 and the WASH complex via the extended C-terminal domain of the FAM21 subunit. These interactions firmly establish the role of highly repetitive sequences in FAM21 for directly engaging both SNX27 and Retromer using distinct but overlapping sequence requirements. LFa repeats consist of two [L/I]F motifs interspersed by tracts of acidic side chains and mediate specific Retromer attachment through VPS35. Notably as this work was under review, a related study provided similar data relating to the Retromer interaction with FAM21 providing further support for the model (51). aDLF repeats consist of a D[L/I]F motif preceded by acidic residues, overlap with the LFa repeats and specifically interact with the FERM domain of SNX27 using a completely different mechanism. Combined with previous work (13, 26, 32), these studies lead to an evolving model for the assembly of the SNX27–Retromer–WASH endosomal recycling domain as one of extreme structural plasticity, sequence redundancy within FAM21, and molecular avidity between FAM21 and assembled oligomers of SNX27–Retromer on the endosomal membrane (**Figure S6**). This network of interactions will also incorporate other proteins known to interact with the FAM21 C-terminus, including the Commander assembly (25, 49, 52, 53), WDR91 (54), RME-8 (55), FKBP15 (13), as well as TBC1D23 which has also been shown to bind to FAM21's LFa repeats (56, 57).

Our data shows that the LFa repeat sequences in FAM21 interact with Retromer at two distinct sites, and this is important for promoting WASH association with Retromer recycling domains, but not strictly essential for recycling of SNX27-Retromer cargos. Opposite to the VPS29-binding surface the VPS35 subunit has two separate sites for binding the peptide motifs, centred on K552, K555, K556 and K559 near the centre of the VPS35 α-helical solenoid (Site 2) and around K701, K705 and K749 near the C-terminus (Site 1). The discovery of two distinct binding pockets was surprising, and points to the potential of both redundancy in motif interactions (each site appears to have similar potential for binding FAM21 repeats) and avidity for increased binding strength (covalently connected sequences in FAM21 binding to two sites simultaneously). The presence of two binding sites is somewhat reminiscent of the binding of bipartite nuclear localisation signals to major and minor surfaces of the α-helical solenoid of importins (58), or of the nuclear receptors with the highly redundant FG repeats in the nucleoporins (59) , although the mechanisms are completely different. Although we do not observe dramatic differences between the affinities of individual and multiple FAM21 repeats for Retromer by ITC, we propose that the combination of Retromer oligomerisation on the membrane (37, 60) with the multivalent nature of FAM21 interactions will promote a high level of specificity in WASH/Retromer engagement (61). Given the enormous extended structure of the FAM21 tail and the number of similar LFa motifs, FAM21 will readily interact with multiple Retromer complexes when organised into polymeric arches at the endosomal membrane. It is also worth noting that this will not lead to a specific stoichiometry for the Retromer/WASH interaction, but rather will promote formation of a heterogeneous and dynamic multivalent network.

In addition to the LFa sequences binding to VPS35, we identified a third binding site on the conserved surface of VPS29 for the final repeat of FAM21 which possesses a DPL sequence. This binds with modest affinity, and is likely inessential for direct Retromer-dependent endosomal recruitment of FAM21 (**Figure**

S5B) (12, 13). We speculate however, that once the WASH complex has bound to Retromer and/or SNX27 that repeat 21 could then act to regulate the association of Retromer with other proteins that bind the same site such as TBC1D5 (39, 62, 63) or ANKRD27 (45) (**Figure S6**).

Retromer, SNX27 and WASH are intimately connected in the endosomal sorting and transport of numerous transmembrane proteins (64-66). The current model is that Retromer, along with SNX cargo adaptors such as SNX3 and SNX27, can establish endosomal retrieval sub-domains and membrane tubules enriched in cargo, and WASH is able to nucleate formation of branched actin filaments via Arp2/3 that enhance membrane tubulation and promote scission (8, 67). The capping-interacting motif (CPI) of FAM21 is responsible for recruiting uncapping dynactin mini-filaments, that then prime the WASH-induced actin branching (68). The first indications that Retromer and WASH cooperate in endosomal recycling demonstrated their colocalization and a direct interaction between the FAM21 C-terminal tail and the Retromer complex (10, 12, 13, 26). These studies also identified the 21 LFa repeats in the FAM21 tail and their importance for Retromer association (26). The C-terminal tail of FAM21 is sufficient for endosomal localisation (13), and Retromer is important for endosomal recruitment of WASH (12, 26, 27, 35, 36), although WASH can also be recruited through Retromer-independent mechanisms via FAM21 and WASHC4/SWIP subunits respectively (50). WASH depletion was also reported to result in exaggerated endosome-derived tubules (9, 10, 69), although this is not universally observed (43, 46, 70, 71).

Previous research established that the FERM domain of SNX27 associates with the aDLF motifs of SNX1 and SNX2 (32, 33), and our data now shows that FAM21 utilises an identical mechanism to engage with the SNX27 adaptor. As shown in **Figure 4F**, the sequence alignment with SNX1/SNX2 peptides shows the D[L/I]F triplet is the most important component for binding, and at least two acidic amino acids before this motif are also important for promoting electrostatic interactions with SNX27. SNX1 and SNX2 are SNX-BAR proteins and subunits of the ESCPE-1 complex along with SNX5 and SNX6 (32). Mutations targeting the aDLF motif in SNX1 or SNX2 that disrupted binding to SNX27 have highlighted the role of the SNX27-ESCPE-1 interaction in promoting the tubular-based endosomal exit and cell surface recycling of SNX27-Retromer cargo (32, 33). The results here both extend these previous analyses and complicate their interpretation, as the SNX27(R498D) FERM domain mutation disrupts not only ESCPE-1 binding but also FAM21 and WASH association. As it is impossible to design SNX27 mutations that only affect SNX1/SNX2 but not FAM21 binding (and *vice versa*), we currently cannot disentangle the individual roles of each interaction on SNX27-dependent trafficking, and effects could be due to either interaction or a combination of both. Overall, however, this further establishes that both Retromer and also SNX27 serve as direct ligands for overlapping multivalent repeat sequences in the FAM21 tail.

Combined with previous studies, our work makes it clear that the formation of endosomal retrieval sub-domains involves a dynamic network of generally low affinity interactions between Retromer, SNX27, ESCPE-1 and the WASH complex (and not discussed here ANKRD50) (44, 46), that includes a series of polyvalent extended sequences in subunits of the ESCPE-1 and WASH complexes. Low affinity interactions ensure that coincidence sensing of cargo and accessory proteins is required to provide the avidity necessary for pathway progression. One could consider these to be 'checks and balances' that derive from an instability

in the protein interaction network when there is insufficient density of cargo and accessory proteins, then sub-domain organisation and coat formation will not be stabilised and the pathway will not progress (72). A more detailed understanding of both the spatial and temporal regulation of the interactions within the SNX27–Retromer–WASH–ESCPE-1 pathway will be challenging due to the high degree of multivalent and low affinity interactions involved, but will be essential for a complete portrait of this endosomal retrieval and recycling pathway(s). Reconstituting this pathway *in vitro* on artificial membranes, as well as high-resolution live-cell imaging will be required to begin to answer these questions, but the work here provides a key mechanistic foundation for these studies.

ACKNOWLEDGEMENTS:

We acknowledge use of the University of Queensland Remote Operation Crystallization and X-ray (UQ ROCX) Facility and the assistance of G.King and K.A.Arachchige. X-ray data were collected on the MX1 and MX2 microfocus beamline at the Australian Synchrotron.

FUNDING:

B.M.C. is supported by an Investigator Grant Project Grant from the National Health and Medical Research Council (APP2016410 and APP1156493). We thank the Bristol Proteomics Facility at the University of Bristol. P.J.C. is supported by the Wellcome Trust (104568/Z/14/Z amd 220260/Z/20/Z), the MRC (MR/L007363/1 and MR/P018807/1), the Lister Institute of Preventive Medicine, and the Royal Society Noreen Murray Research Professorship (RSRP/R1/211004). A.P.J. was funded through an MRC PhD Studentship.

AUTHOR CONTRIBUTIONS:

Initial Concept: B.M.C., and P.J.C.

Concept development: all authors.

ITC and structural determination and analysis: Q.G. and K.C.

Biochemistry and cell biology analysis: M.G-A., A.P.J., B.S., and C.M.D.

Proteomic analysis: K.J.H.

Data analysis and Figure generation: Q.G., K.C., A.P.J., B.S., and M.G-A.

Funding acquisition: B.M.C., and P.J.C.

Supervision: B.M.C., and P.J.C.

Writing – 1st draft: Q.G. and K.C.

(Writing – review & editing: all authors)

CONFLICTS OF INTEREST:

The authors declare that they have no conflict of interest.

399 **MATERIALS AND METHODS**

400 Detailed methods are provided in the **Supporting Information Appendix**. DNA constructs, antibodies and
401 other reagents used in this study are described in the **Supporting Information Appendix** and **Table S5.** All
402 proteins used in this work were recombinantly expressed in *Eschericia coli* and purified using standard affinity
403 chromatography and size exclusion chromatography. ITC experiments were performed using a MicroCal
404 PEAQ ITC instrument operating at 25ºC. Crystallographic X-ray diffraction data was collected at the
405 Australian Synchrotron with structures determined by molecular replacement as outlined in **Table S2 and S4.**
406 AlphaFold2 (73) predictions were performed using the open-source ColabFold pipeline (74). HeLa, HEK-
407 293T and H4 cell lines were sourced from and authenticated by ATCC. Cells were grown under standard
408 conditions in DMEM (Sigma-Aldrich) supplemented with 10% (v/v) FCS (Sigma-Aldrich) and 1%
409 penicillin/streptomycin (Gibco, USA). Statistics for western blots and confocal microscopy images were
410 calculated from a minimum of 3 independent experimental repeats.

411 **FIGURES**

412 **Figure 1. Retromer VPS29 is responsible for binding to repeat 21 of FAM21.**

413 (**A**) Schematic diagram showing features of human FAM21, and highlighting the 21 LFa repeats in the
414 unstructured tail. (**B**) Sequences of the 21 LFa repeats within the FAM21 tail. Conserved [I/L]F residues are
415 shown in grey and acidic residues are in red. The PL residues of repeat 21 are highlighted in green. (**C**) ITC
416 thermograms showing the titration of Retromer, the VPS29–VPS35$_{481-796}$ subcomplex, and VPS29 alone with
417 FAM21$_{R19}$ (blue); FAM21$_{R20}$ (green); and FAM21$_{R21}$ (red) peptides. (**D**) Retromer shows binding to GST-
418 FAM21$_{R19-R20}$. (**E**) VPS29 and FAM21$_{R21}$ peptide interaction can be blocked by the addition of the PL-
419 sequence containing cyclic peptide RT-D1. All ITC graphs show the integrated (bottom) and normalized raw
420 data (top) fit with a single-site binding model.

421

422 **Figure 2. Structural basis for the interaction of LFa repeats with Retromer subunit VPS35.**

423 (**A**) Overall crystal structure of VPS29–VPS35$_{481-796}$ in complex with FAM21$_{R20}$ peptides showing both
424 complexes from the asymmetric unit. (**B**) VPS35 is highly conserved in the FAM21$_{R20}$ binding region. The
425 density corresponding to the FAM21$_{R20}$ peptide is shown in mesh using 2Fo–Fc map contoured at 1σ. Sequence
426 conservation of VPS35 was mapped with CONSURF (75). (**C**) The electrostatic surface map showing
427 FAM21$_{R20}$ binding location on VPS35. (**D**) Predicted alignment Error (PAE) plots of VPS29–VPS35$_{481-796}$–
428 FAM21$_{R19-R20}$ complexes generated by Alphafold2. (**E**) The predicted structure highlighting the per-residue
429 confidence score (pLDDT) between 0 to 100. Regions showing low pLDDT score (green and orange) are
430 likely to be unstructured. (**F**) Alignment of the Alphafold2 model of FAM21$_{R20}$ (cyan) and the crystal structure
431 (VPS35 in light purple, FAM21$_{R20}$ as light pink) highlighting the key interacting residues between FAM21$_{R20}$
432 and VPS35. The insert shows the refined electron density of the FAM21$_{R20}$ peptide observed in the crystal
433 structure. (**G**) Co-immunoprecipitation (co-IP) of C-terminal GFP-tagged VPS35mutants in the Site 2 binding
434 pocket in HEK293T cells. (**H**) Co-IP of C-terminal GFP-tagged VPS35 and mutants in the Site 1 binding
435 pocket. Quantitation of these Western blots is shown in **Figure S2.** (**I**) ITC analysis showing the binding of
436 GST-FAM21$_{R19-R20}$ with either native Retromer or VPS35 (K555N/K556L/K559Q) Site 2 mutant. All ITC
437 graphs show the integrated (bottom) and normalized raw data (top) fit with a single-site binding model. (**J**)
438 The locations of the Site 1 and Site 2 FAM21 repeat binding sites are shown in the context of the VPS35-
439 mediated Retromer dimer assembly derived from cryoelectron tomography (37). The location of the D620N
440 mutation linked to Parkinson's Disease is also indicated in cyan spheres.

441

442 **Figure 3. Structural basis for repeat 21 binding to VPS29 and model for Retromer engagement by**
443 **multiple FAM21 repeats.**

444 (**A**) Crystal structure of VPS29–VPS35$_{481-796}$ bound to the FAM21$_{R21}$ peptide. (**B**) Crystal structure of VPS29
445 in complex with FAM21$_{R21}$ peptide. (**C**) Enlarged view highlighting the refined density of FAM21$_{R21}$ peptide
446 peptide (2Fo–Fc map contoured at 1σ). (**D**) Structural alignment of the VPS29–FAM21$_{R21}$ peptide complex
447 with the VPS29–RT-D1 cyclic peptide complex (PDB ID 6XS5)(34) highlighting the PL motif binding region.
448 (**E**) Predicted alignment Error (PAE) plots showing the predicted structure of VPS29–VPS35$_{481-796}$–FAM21$_{R19-}$

$_{R21}$ complex generated by Alphafold2. (**F**) The predicted structure highlighting the per-residue confidence score (pLDDT) between 0 to 100. Regions showing low pLDDT score (represents as green and orange) are likely to be unstructured. (**G**) Superimposition of all the two crystal structures with the Alphafold2 model. (**H**) Alphafold2 predictions of the complex of VPS29–VPS35 with either FAM21$_{R1-R2}$, FAM21$_{R3-R4}$ or FAM21$_{R15-R16}$ showing pairs of repeats predicted to bind to the same positively charged grooves as repeats FAM21$_{19-20}$. (**I**) ITC thermogram showing the binding between Retromer with FAM21$_{R5}$ (red line), FAM21$_{R15}$ (blue line) and FAM21$_{R17}$ (green) peptides. All ITC graphs show the integrated (right) and normalized raw data (left) fit with a single-site binding model. (**J**) The locations of the FAM21 repeat 19 and 20 binding sites as well as the VPS29-binding repeat 21 are shown in the context of the VPS35-mediated Retromer dimer assembly derived from cryoelectron tomography (37) (PDB ID: 7BLN). The right panel shows two proposed binding models for how FAM21 can bind to a Retromer dimer in *cis* or *trans*.

Figure 4. FAM21 aDLF repeats also binds to the SNX27 FERM domain.

(**A**) Co-IP of GFP-tagged FAM21 tail in HEK293T cells. Samples were analysed by quantitative fluorescence-based western blotting. The band intensities of SNX27 and VPS35 were measured from n=3 independent experiments using Odyssey software. The SNX27 and VPS35 band intensities, normalized to GFP expression, are presented as the average fraction of the full length FAM21 tail. (**B**) ITC analysis showing the binding between GST-FAM21$_{R19-21}$ and SNX27 (yellow line) and SNX27 FERM (blue line). (**C**) Similar binding experiment showing the binding of FAM21 peptides FAM21$_{R19}$, FAM21$_{R20}$ and FAM21$_{R21}$ with either (**C**) SNX27 FL or (**D**) SNX27 FERM. (**E**) ITC thermogram comparing the binding between native FAM21$_{R20}$ and ^{1298}IF^{1299} to SS mutant peptides with SNX27 FL. (**F**) List of FAM21 peptides containing the same aDLF motif to those observed in SNX1 and SNX2. (**G**) ITC binding curves of the FAM21$_{R5}$, FAM21$_{R8}$ and FAM21$_{R17}$ peptides titrated into either (**G**) SNX27 FL or (**H**) SNX27 FERM. All ITC graphs show the integrated (bottom) and normalized raw data (top) fit with a single-site binding model.

Figure 5. Structural basis for SNX27 interaction with FAM21 aDLF repeats.

(**A**) Crystal structures of the SNX27 FERM domain bound to aDLF repeats of FAM21. Top views show the key region of SNX27 FERM involved in the binding to the FAM21 aDLF seqeunces (**A**) FAM21$_{R15}$, (**B**) FAM21$_{R19}$ and (**C**) FAM21$_{R20}$. Middle panels show the electron density corresponding to a simulated-annealing composite omit 2Fo–Fc map contoured at 1σ. Bottom panels show electrostatic surface potential of SNX27 highlighting the positively charged pocket of SNX27 FERM. (**D**) Structural alignment showing the high degree of similarity between all three complex structures. (**E**) Sequence conservation map highlighting the conserved pocket of SNX27 FERM domain for binding to FAM21 aDLF motifs. (**F**) Structural alignment of SNX27 bound to FAM21$_{R19}$ with the SNX27–SNX1$_{75-92}$ complex (PDB ID 7CT1; (33)) showing they bind the same pocket. (**G**) ITC analysis showing the binding of the FAM21$_{R19}$ peptide with the native or mutant forms of SNX27. The ITC graphs represent the integrated and normalized data fit with 1:1 ratio binding. (**H**) Co-IP of GFP-SNX27 mutants and binding of WASH, Retromer and ESCPE-1 (represented by SNX6) proteins assessed by Western blot. (**I**) Proteomic studies comparing the native SNX27 and mutated SNX27 R498D

binding capabilities with SNX27 interactors assessed by Co-IP (n = 6; derived from 2 biological repeats each with 3 technical repeats). Mutation of the aDLF binding pocket causes disrupted interactions with most WASH and ESCPE-1 subunits. The full list of detected proteins is provided in **Dataset S1**.

Figure 6. VPS35 interaction with FAM21 contributes to its endosomal localization, but it is not strictly required for SNX27–Retromer recycling.

(**A**) VPS35 KO HeLa cells show a reduction in the colocalisation of FAM21 to SNX1-positive endosomal domains. Re-expression of VPS35-GFP WT can partially rescue this mislocalization, but the mutant VPS35(NLQE)-GFP with both FAM21 binding sites mutated is unable to restore FAM21 recruitment levels. A total of 90 cells were analyzed in each condition for colocalization between SNX1 and FAM21 across n=3 independent experiments. Scale bars, 25 µm (micrographs) and 5 µm (magnified images). (**B**) VPS35 KO HeLa cells showed reduced cell surface levels of SNX27–Retromer dependent cargos including GLUT1 and KIDINS220. VPS35 KO clonal line was stably transduced with lentiviral particles containing VPS35-GFP WT or VPS35(NLQE)-GFP. Re-expression and rescue with both constructs is able to rescue the cell surface levels of these cargos. This indicates that full binding of FAM21 to VPS35 is not strictly required for SNX27–Retromer mediated endosomal recycling. (**C**) Quantitation of Western blots is shown. Similar results were obtained in H4 cell lines as shown in **Figure S5C**. Statistics for western blots and confocal microscopy images were calculated from a minimum of 3 independent experimental repeats Graphs were plotted representing the mean value ± the standard error (SE) for each experimental condition. s. In all graphs, * = $p < 0.05$, ** = $p < 0.01$, *** = $p < 0.001$, **** = $p < 0.0001$.

510 **REFERENCES:**

511

512 1. P. J. Cullen, F. Steinberg, To degrade or not to degrade: mechanisms and significance of endocytic
513 recycling. *Nat Rev Mol Cell Biol* **19**, 679-696 (2018).

514 2. C. Burd, P. J. Cullen, Retromer: a master conductor of endosome sorting. *Cold Spring Harb Perspect*
515 *Biol* **6** (2014).

516 3. K. E. Chen, M. D. Healy, B. M. Collins, Towards a molecular understanding of endosomal trafficking
517 by Retromer and Retriever. *Traffic* **20**, 465-478 (2019).

518 4. T. Clairfeuille *et al.*, A molecular code for endosomal recycling of phosphorylated cargos by the
519 SNX27-retromer complex. *Nat Struct Mol Biol* **23**, 921-932 (2016).

520 5. M. Gallon *et al.*, A unique PDZ domain and arrestin-like fold interaction reveals mechanistic details
521 of endocytic recycling by SNX27-retromer. *Proc Natl Acad Sci U S A* **111**, E3604-3613 (2014).

522 6. M. L. Lunn *et al.*, A unique sorting nexin regulates trafficking of potassium channels via a PDZ
523 domain interaction. *Nat Neurosci* **10**, 1249-1259 (2007).

524 7. F. Steinberg *et al.*, A global analysis of SNX27-retromer assembly and cargo specificity reveals a
525 function in glucose and metal ion transport. *Nat Cell Biol* **15**, 461-471 (2013).

526 8. P. Temkin *et al.*, SNX27 mediates retromer tubule entry and endosome-to-plasma membrane
527 trafficking of signalling receptors. *Nat Cell Biol* **13**, 715-721 (2011).

528 9. E. Derivery *et al.*, The Arp2/3 activator WASH controls the fission of endosomes through a large
529 multiprotein complex. *Dev Cell* **17**, 712-723 (2009).

530 10. T. S. Gomez, D. D. Billadeau, A FAM21-containing WASH complex regulates retromer-dependent
531 sorting. *Dev Cell* **17**, 699-711 (2009).

532 11. T. S. Gomez, J. A. Gorman, A. A. de Narvajas, A. O. Koenig, D. D. Billadeau, Trafficking defects in
533 WASH-knockout fibroblasts originate from collapsed endosomal and lysosomal networks. *Mol Biol*
534 *Cell* **23**, 3215-3228 (2012).

535 12. M. E. Harbour *et al.*, The cargo-selective retromer complex is a recruiting hub for protein complexes
536 that regulate endosomal tubule dynamics. *J Cell Sci* **123**, 3703-3717 (2010).

537 13. M. E. Harbour, S. Y. Breusegem, M. N. Seaman, Recruitment of the endosomal WASH complex is
538 mediated by the extended 'tail' of Fam21 binding to the retromer protein Vps35. *Biochem J* **442**, 209-
539 220 (2012).

540 14. D. Jia *et al.*, WASH and WAVE actin regulators of the Wiskott-Aldrich syndrome protein (WASP)
541 family are controlled by analogous structurally related complexes. *Proc Natl Acad Sci U S A* **107**,
542 10442-10447 (2010).

543 15. P. N. Valdmanis *et al.*, Mutations in the KIAA0196 gene at the SPG8 locus cause hereditary spastic
544 paraplegia. *Am J Hum Genet* **80**, 152-161 (2007).

545 16. S. B. Padrick, M. K. Rosen, Physical mechanisms of signal integration by WASP family proteins.
546 *Annu Rev Biochem* **79**, 707-735 (2010).

547 17. L. E. Burianek, S. H. Soderling, Under lock and key: spatiotemporal regulation of WASP family
548 proteins coordinates separate dynamic cellular processes. *Semin Cell Dev Biol* **24**, 258-266 (2013).

549 18. S. N. Duleh, M. D. Welch, WASH and the Arp2/3 complex regulate endosome shape and trafficking.
550 *Cytoskeleton (Hoboken)* **67**, 193-206 (2010).

19. M. Park, H. J. Kim, B. Lim, A. Wylegala, M. Toborek, Methamphetamine-induced occludin endocytosis is mediated by the Arp2/3 complex-regulated actin rearrangement. *J Biol Chem* **288**, 33324-33334 (2013).

20. R. Chakrabarti, M. Lee, H. N. Higgs, Multiple roles for actin in secretory and endocytic pathways. *Curr Biol* **31**, R603-R618 (2021).

21. S. T. de Bot *et al.*, Pure adult-onset spastic paraplegia caused by a novel mutation in the KIAA0196 (SPG8) gene. *J Neurol* **260**, 1765-1769 (2013).

22. F. Ropers *et al.*, Identification of a novel candidate gene for non-syndromic autosomal recessive intellectual disability: the WASH complex member SWIP. *Hum Mol Genet* **20**, 2585-2590 (2011).

23. B. N. Vardarajan *et al.*, Identification of Alzheimer disease-associated variants in genes that regulate retromer function. *Neurobiol Aging* **33**, 2231 e2215-2231 e2230 (2012).

24. B. E. Lauffer *et al.*, SNX27 mediates PDZ-directed sorting from endosomes to the plasma membrane. *J Cell Biol* **190**, 565-574 (2010).

25. K. E. McNally *et al.*, Retriever is a multiprotein complex for retromer-independent endosomal cargo recycling. *Nat Cell Biol* **19**, 1214-1225 (2017).

26. D. Jia, T. S. Gomez, D. D. Billadeau, M. K. Rosen, Multiple repeat elements within the FAM21 tail link the WASH actin regulatory complex to the retromer. *Mol Biol Cell* **23**, 2352-2361 (2012).

27. E. Helfer *et al.*, Endosomal recruitment of the WASH complex: active sequences and mutations impairing interaction with the retromer. *Biol Cell* **105**, 191-207 (2013).

28. B. Balana *et al.*, Mechanism underlying selective regulation of G protein-gated inwardly rectifying potassium channels by the psychostimulant-sensitive sorting nexin 27. *Proc Natl Acad Sci U S A* **108**, 5831-5836 (2011).

29. R. Ghai *et al.*, Phox homology band 4.1/ezrin/radixin/moesin-like proteins function as molecular scaffolds that interact with cargo receptors and Ras GTPases. *Proc Natl Acad Sci U S A* **108**, 7763-7768 (2011).

30. R. Ghai *et al.*, Phosphoinositide binding by the SNX27 FERM domain regulates its localization at the immune synapse of activated T-cells. *J Cell Sci* **128**, 553-565 (2015).

31. Y. Li, S. Liao, F. Li, Z. Zhu, Crystal Structure of the PX Domain of SNX27. *Biochemistry (Mosc)* **84**, 147-152 (2019).

32. B. Simonetti *et al.*, SNX27-Retromer directly binds ESCPE-1 to transfer cargo proteins during endosomal recycling. *PLoS Biol* **20**, e3001601 (2022).

33. X. Yong *et al.*, SNX27-FERM-SNX1 complex structure rationalizes divergent trafficking pathways by SNX17 and SNX27. *Proc Natl Acad Sci U S A* **118** (2021).

34. K. E. Chen *et al.*, De novo macrocyclic peptides for inhibiting, stabilizing, and probing the function of the retromer endosomal trafficking complex. *Sci Adv* **7**, eabg4007 (2021).

35. I. J. McGough *et al.*, Retromer binding to FAM21 and the WASH complex is perturbed by the Parkinson disease-linked VPS35(D620N) mutation. *Curr Biol* **24**, 1670-1676 (2014).

36. E. Zavodszky *et al.*, Mutation in VPS35 associated with Parkinson's disease impairs WASH complex association and inhibits autophagy. *Nat Commun* **5**, 3828 (2014).

590 37. N. Leneva, O. Kovtun, D. R. Morado, J. A. G. Briggs, D. J. Owen, Architecture and mechanism of
591 metazoan retromer:SNX3 tubular coat assembly. *Sci Adv* **7** (2021).

592 38. M. Romano-Moreno *et al.*, Molecular mechanism for the subversion of the retromer coat by the
593 Legionella effector RidL. *Proc Natl Acad Sci U S A* **114**, E11151-E11160 (2017).

594 39. D. Jia *et al.*, Structural and mechanistic insights into regulation of the retromer coat by TBC1d5. *Nat*
595 *Commun* **7**, 13305 (2016).

596 40. D. J. Boesch *et al.*, Structural Organization of the Retriever-CCC Endosomal Recycling Complex.
597 *bioRxiv* 10.1101/2023.06.06.543888, 2023.2006.2006.543888 (2023).

598 41. M. D. Healy *et al.*, Structure of the endosomal Commander complex linked to Ritscher-Schinzel
599 syndrome. *Cell* **186**, 2219-2237 e2229 (2023).

600 42. S. Laulumaa, E.-P. Kumpula, J. T. Huiskonen, M. Varjosalo, Structure and Interactions of the
601 Endogenous Human Commander Complex. *bioRxiv* 10.1101/2023.04.03.535349,
602 2023.2004.2003.535349 (2023).

603 43. S. Lee, J. Chang, C. Blackstone, FAM21 directs SNX27-retromer cargoes to the plasma membrane by
604 preventing transport to the Golgi apparatus. *Nat Commun* **7**, 10939 (2016).

605 44. A. Kvainickas *et al.*, Retromer- and WASH-dependent sorting of nutrient transporters requires a
606 multivalent interaction network with ANKRD50. *J Cell Sci* **130**, 382-395 (2017).

607 45. H. Crawley-Snowdon *et al.*, Mechanism and evolution of the Zn-fingernail required for interaction of
608 VARP with VPS29. *Nat Commun* **11**, 5031 (2020).

609 46. I. J. McGough *et al.*, Identification of molecular heterogeneity in SNX27-retromer-mediated
610 endosome-to-plasma-membrane recycling. *J Cell Sci* **127**, 4940-4953 (2014).

611 47. A. Kvainickas *et al.*, Cargo-selective SNX-BAR proteins mediate retromer trimer independent
612 retrograde transport. *J Cell Biol* **216**, 3677-3693 (2017).

613 48. B. Simonetti, C. M. Danson, K. J. Heesom, P. J. Cullen, Sequence-dependent cargo recognition by
614 SNX-BARs mediates retromer-independent transport of CI-MPR. *J Cell Biol* **216**, 3695-3712 (2017).

615 49. A. Singla *et al.*, Endosomal PI(3)P regulation by the COMMD/CCDC22/CCDC93 (CCC) complex
616 controls membrane protein recycling. *Nat Commun* **10**, 4271 (2019).

617 50. V. Dostal, T. Humhalova, P. Berankova, O. Pacalt, L. Libusova, SWIP mediates retromer-independent
618 membrane recruitment of the WASH complex. *Traffic* **24**, 216-230 (2023).

619 51. M. Romano-Moreno, E. N. Astorga-Simón, A. L. Rojas, A. Hierro, Retromer-mediated recruitment of
620 the WASH complex involves discrete interactions between VPS35, VPS29, and FAM21. *Protein Sci*
621 **33**, e4980 (2024).

622 52. P. Bartuzi *et al.*, CCC- and WASH-mediated endosomal sorting of LDLR is required for normal
623 clearance of circulating LDL. *Nat Commun* **7**, 10961 (2016).

624 53. C. A. Phillips-Krawczak *et al.*, COMMD1 is linked to the WASH complex and regulates endosomal
625 trafficking of the copper transporter ATP7A. *Mol Biol Cell* **26**, 91-103 (2015).

626 54. N. Liu, K. Liu, C. Yang, WDR91 specifies the endosomal retrieval subdomain for retromer-dependent
627 recycling. *J Cell Biol* **221** (2022).

628 55. C. L. Freeman, G. Hesketh, M. N. Seaman, RME-8 coordinates the activity of the WASH complex
629 with the function of the retromer SNX dimer to control endosomal tubulation. *J Cell Sci* **127**, 2053-
630 2070 (2014).

631 56. W. Huang *et al.*, Structural and functional studies of TBC1D23 C-terminal domain provide a link
632 between endosomal trafficking and PCH. *Proc Natl Acad Sci U S A* **116**, 22598-22608 (2019).

633 57. J. J. H. Shin, A. K. Gillingham, F. Begum, J. Chadwick, S. Munro, TBC1D23 is a bridging factor for
634 endosomal vesicle capture by golgins at the trans-Golgi. *Nat Cell Biol* **19**, 1424-1432 (2017).

635 58. M. Christie *et al.*, Structural Biology and Regulation of Protein Import into the Nucleus. *J Mol Biol*
636 **428**, 2060-2090 (2016).

637 59. R. H. Kehlenbach, P. Neumann, R. Ficner, A. Dickmanns, Interaction of nucleoporins with nuclear
638 transport receptors: a structural perspective. *Biol Chem* **404**, 791-805 (2023).

639 60. O. Kovtun *et al.*, Structure of the membrane-assembled retromer coat determined by cryo-electron
640 tomography. *Nature* **561**, 561-564 (2018).

641 61. K. Teilum, J. G. Olsen, B. B. Kragelund, On the specificity of protein-protein interactions in the
642 context of disorder. *Biochem J* **478**, 2035-2050 (2021).

643 62. M. N. Seaman, M. E. Harbour, D. Tattersall, E. Read, N. Bright, Membrane recruitment of the cargo-
644 selective retromer subcomplex is catalysed by the small GTPase Rab7 and inhibited by the Rab-GAP
645 TBC1D5. *J Cell Sci* **122**, 2371-2382 (2009).

646 63. M. N. J. Seaman, A. S. Mukadam, S. Y. Breusegem, Inhibition of TBC1D5 activates Rab7a and can
647 enhance the function of the retromer cargo-selective complex. *J Cell Sci* **131** (2018).

648 64. A. I. Fokin, A. M. Gautreau, Assembly and Activity of the WASH Molecular Machine: Distinctive
649 Features at the Crossroads of the Actin and Microtubule Cytoskeletons. *Front Cell Dev Biol* **9**, 658865
650 (2021).

651 65. B. Simonetti, P. J. Cullen, Actin-dependent endosomal receptor recycling. *Curr Opin Cell Biol* **56**, 22-
652 33 (2019).

653 66. M. N. Seaman, A. Gautreau, D. D. Billadeau, Retromer-mediated endosomal protein sorting: all
654 WASHed up! *Trends Cell Biol* **23**, 522-528 (2013).

655 67. M. A. Puthenveedu *et al.*, Sequence-dependent sorting of recycling proteins by actin-stabilized
656 endosomal microdomains. *Cell* **143**, 761-773 (2010).

657 68. A. I. Fokin *et al.*, The Arp1/11 minifilament of dynactin primes the endosomal Arp2/3 complex. *Sci*
658 *Adv* **7** (2021).

659 69. P. V. Ryder *et al.*, The WASH complex, an endosomal Arp2/3 activator, interacts with the Hermansky-
660 Pudlak syndrome complex BLOC-1 and its cargo phosphatidylinositol-4-kinase type IIalpha. *Mol Biol*
661 *Cell* **24**, 2269-2284 (2013).

662 70. C. M. Buckley *et al.*, WASH drives early recycling from macropinosomes and phagosomes to maintain
663 surface phagocytic receptors. *Proc Natl Acad Sci U S A* **113**, E5906-E5915 (2016).

664 71. H. E. Miller, C. L. Larson, R. A. Heinzen, Actin polymerization in the endosomal pathway, but not on
665 the Coxiella-containing vacuole, is essential for pathogen growth. *PLoS Pathog* **14**, e1007005 (2018).

666 72. E. M. Schmid, H. T. McMahon, Integrating molecular and network biology to decode endocytosis.
667 *Nature* **448**, 883-888 (2007).

73. J. Jumper *et al.*, Highly accurate protein structure prediction with AlphaFold. *Nature* **596**, 583-589 (2021).

74. M. Mirdita *et al.*, ColabFold: making protein folding accessible to all. *Nat Methods* **19**, 679-682 (2022).

75. H. Ashkenazy *et al.*, ConSurf 2016: an improved methodology to estimate and visualize evolutionary conservation in macromolecules. *Nucleic Acids Res* **44**, W344-350 (2016).

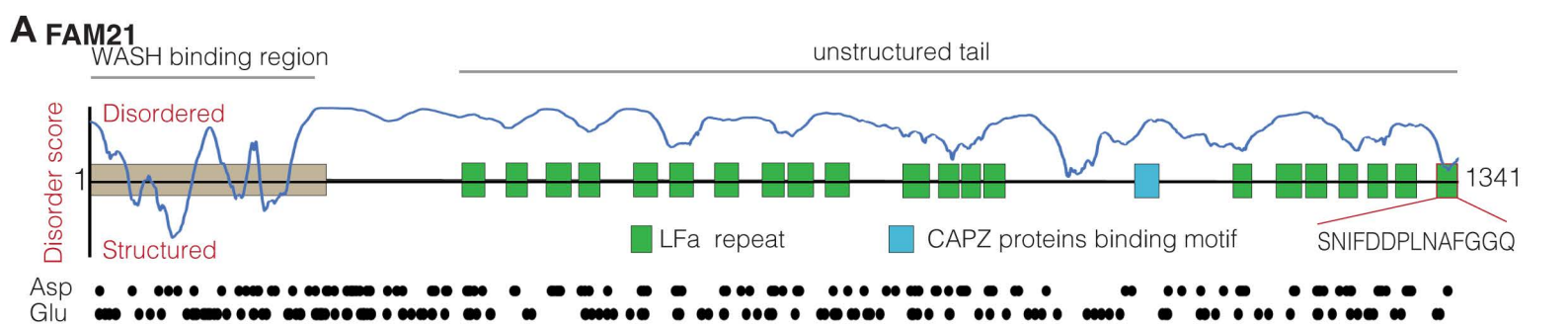

B

FAM21 repeat	Range	LFa sequence	FAM21 repeat	Range	LFa sequence
R1	367–378	LFDDEDEESDLF	R12	839–847	VFQDEELLF
R2	411–419	VFLGDTDVF	R13	856–862	DPDVDLF
R3	450–463	LFDDDDGDDDDDFF	R14	878–888	LFGDDEDDDLF
R4	482–491	IFGDEEGDLF	R15	1129–1136	LFDSGDIF
R5	537–548	LFSDEEDSEDLF	R16	1171–1185	MFPALGEASSDDDLF
R6	572–583	LFDDEDEEDNLF	R17	1201–1209	LLEDEDDLF
R7	617–629	LFSSDEEDQWNIP	R18	1234–1240	IFEDDIF
R8	664–674	LFEEDEEDDLF	R19	1262–1270	LFDDNIDIF
R9	690–702	LFEDDVDSGGSLF	R20	1290–1297	IFDDDMDDIF
R10	726–737	LFSDEEEKEAQLG	R21	1330–1338	IFDDPLNAF
R11	803–817	LFDEEEDKMEDQNII			

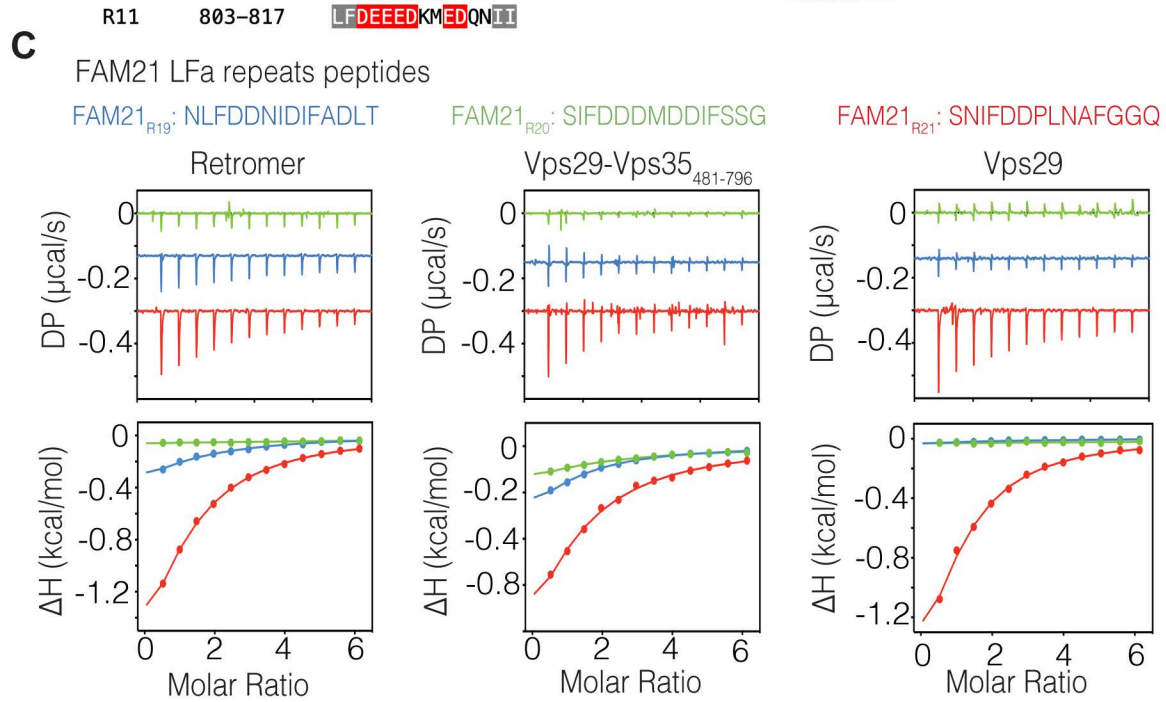

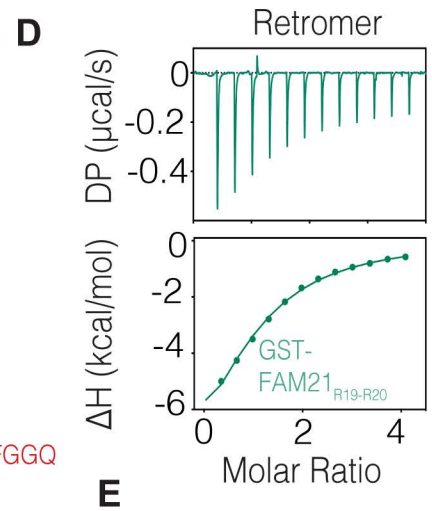

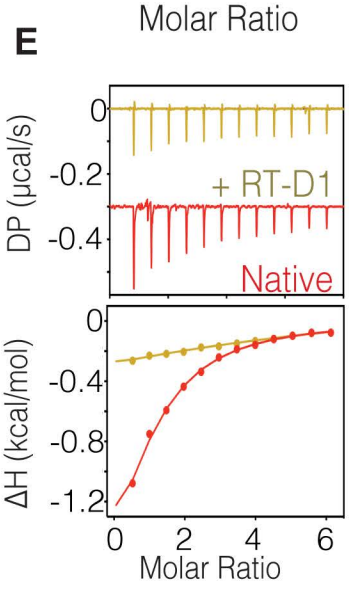

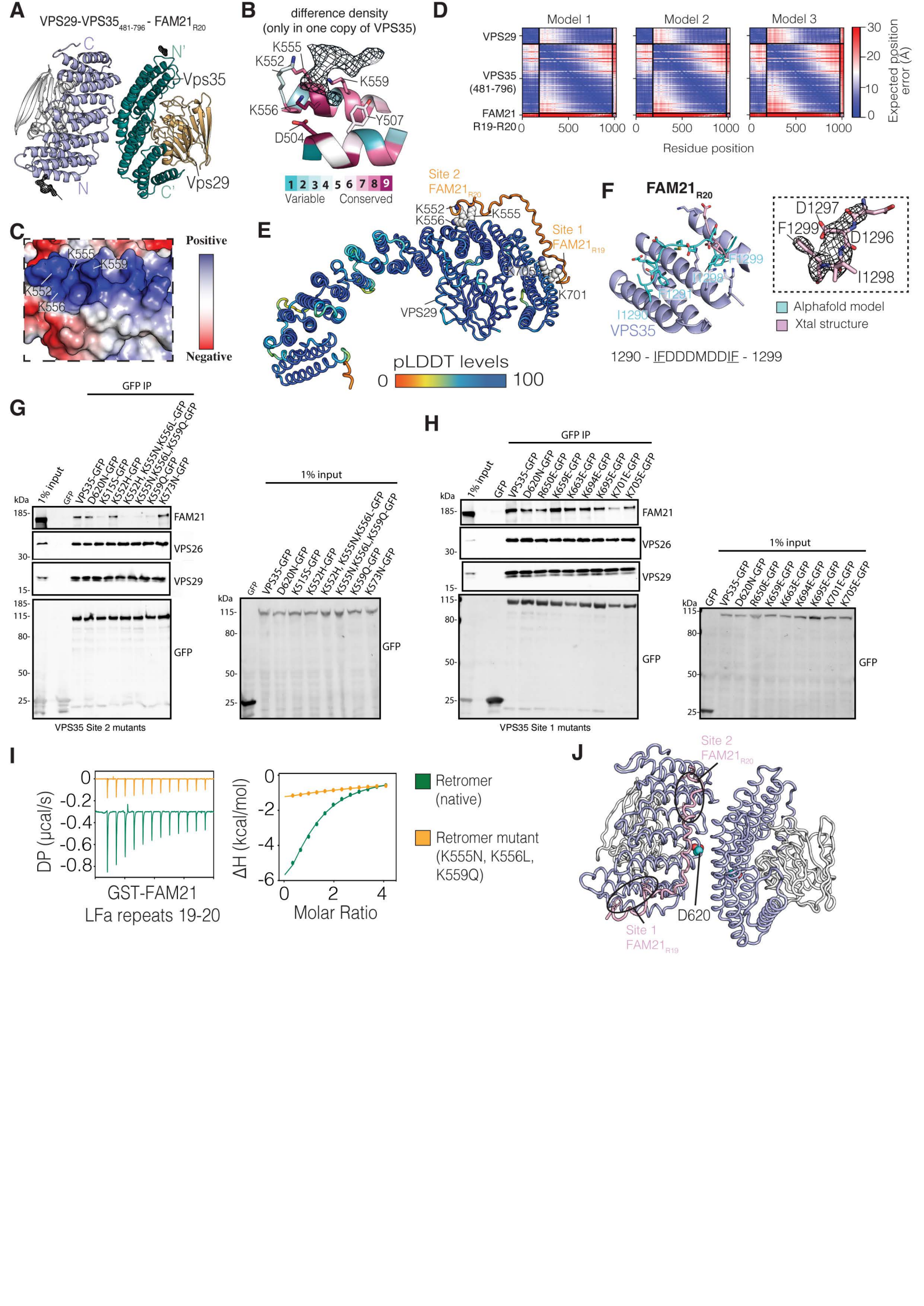
A
VPS29-VPS35481-796 - FAM21R20
C
N'
Vps35
N
C'
Vps29
B
difference density
(only in one copy of VPS35)
K555
K552
K559
K556
Y507
D504
1 2 3 4 5 6 7 8 9
Variable
Conserved
D
Model 1
Model 2
Model 3
VPS29
VPS35
(481-796)
FAM21
R19-R20
0
500
1000
Residue position
Expected position error (Å)
30
20
10
0
C
Positive
Negative
K555
K559
K552
K556
E
Site 2
FAM21R20
K552
K556
K555
Site 1
FAM21R19
K705
K701
VPS29
pLDDT levels
0
100
F
FAM21R20
F1299
I1298
F1291
I1290
VPS35
D1297
F1299
D1296
I1298
Alphafold model
Xtal structure
1290 - IFDDDMDDIF - 1299
G
GFP IP
1% input
GFP
VPS35-GFP
D620N-GFP
K515S-GFP
K552H-GFP
K552H, K555N,K556L-GFP
K555N,K556L,K559Q-GFP
K559Q-GFP
K573N-GFP
kDa
185-
30-
15-
115-
80-
50-
25-
FAM21
VPS26
VPS29
GFP
VPS35 Site 2 mutants
H
GFP IP
1% input
GFP
VPS35-GFP
D620N-GFP
R650E-GFP
K659E-GFP
K663E-GFP
K694E-GFP
K695E-GFP
K701E-GFP
K705E-GFP
FAM21
VPS26
VPS29
GFP
VPS35 Site 1 mutants
I
DP (µcal/s)
0
-0.2
-0.4
-0.6
-0.8
GST-FAM21
LFa repeats 19-20
ΔH (kcal/mol)
0
-2
-4
-6
0
2
4
Molar Ratio
Retromer
(native)
Retromer mutant
(K555N, K556L,
K559Q)
J
Site 2
FAM21R20
D620
Site 1
FAM21R19

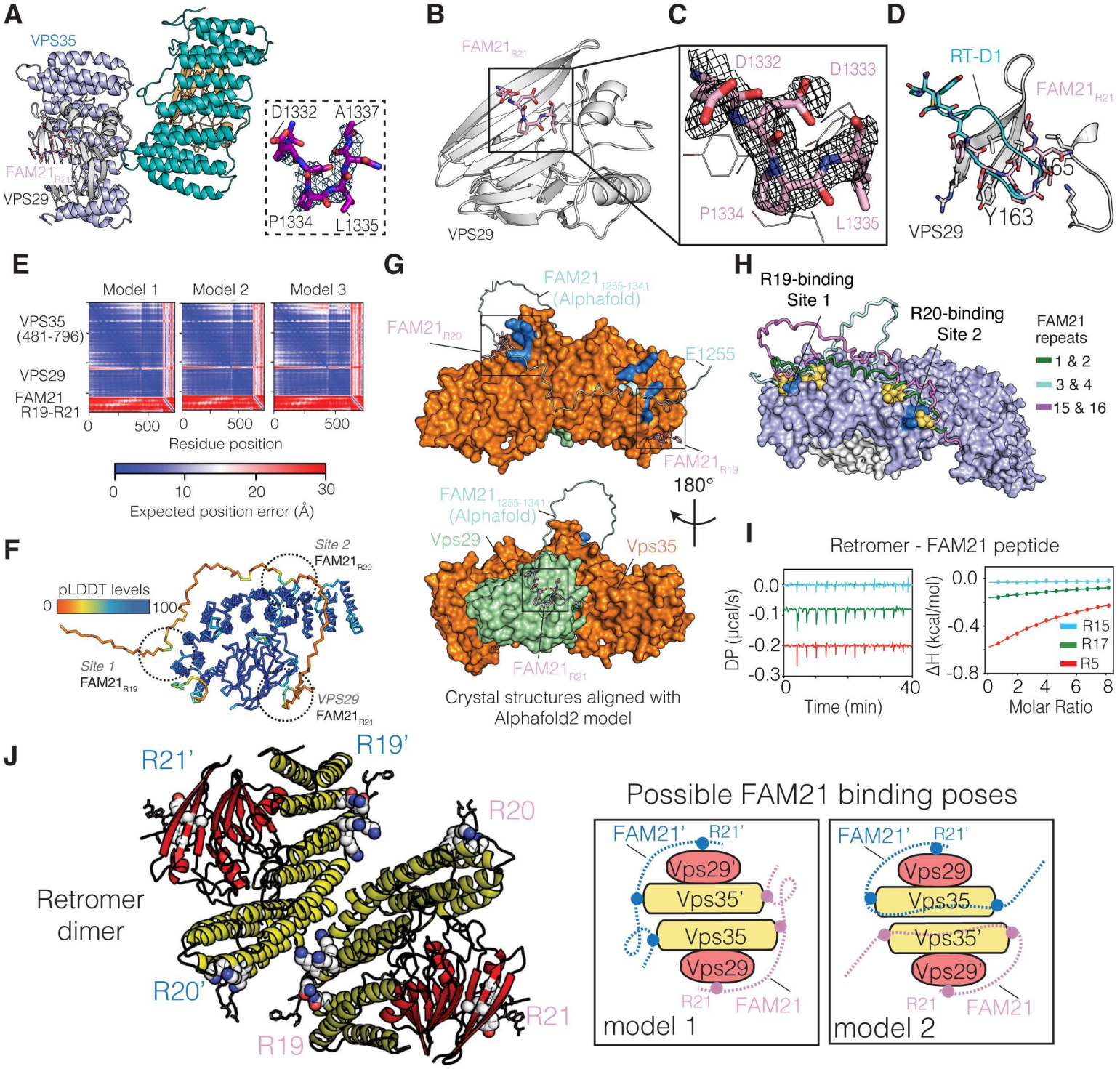
A
VPS35
FAM21R21
VPS29
D1332
A1337
P1334
L1335
B
FAM21R21
VPS29
C
D1332
D1333
P1334
L1335
D
RT-D1
FAM21R21
Y165
Y163
VPS29
E
Model 1
Model 2
Model 3
VPS35 (481-796)
VPS29
FAM21 R19-R21
0
500
Residue position
0
10
20
30
Expected position error (Å)
F
Site 2
FAM21R20
pLDDT levels
0
100
Site 1
FAM21R19
VPS29
FAM21R21
G
FAM21 1255-1341 (Alphafold)
FAM21R20
E1255
FAM21R19
180°
FAM21 1255-1341 (Alphafold)
Vps29
Vps35
FAM21R21
Crystal structures aligned with Alphafold2 model
H
R19-binding Site 1
R20-binding Site 2
FAM21 repeats
1 & 2
3 & 4
15 & 16
I
Retromer - FAM21 peptide
DP (µcal/s)
0.0
-0.1
-0.2
-0.3
0
40
Time (min)
ΔH (kcal/mol)
0.0
-0.4
-0.8
0
2
4
6
8
Molar Ratio
R15
R17
R5
J
R21'
R19'
R20
Retromer dimer
R20'
R21
R19
Possible FAM21 binding poses
FAM21'
R21'
Vps29'
Vps35'
Vps35
Vps29
R21
FAM21
model 1
FAM21'
R21'
Vps29
Vps35
Vps35'
Vps29'
R21
FAM21
model 2

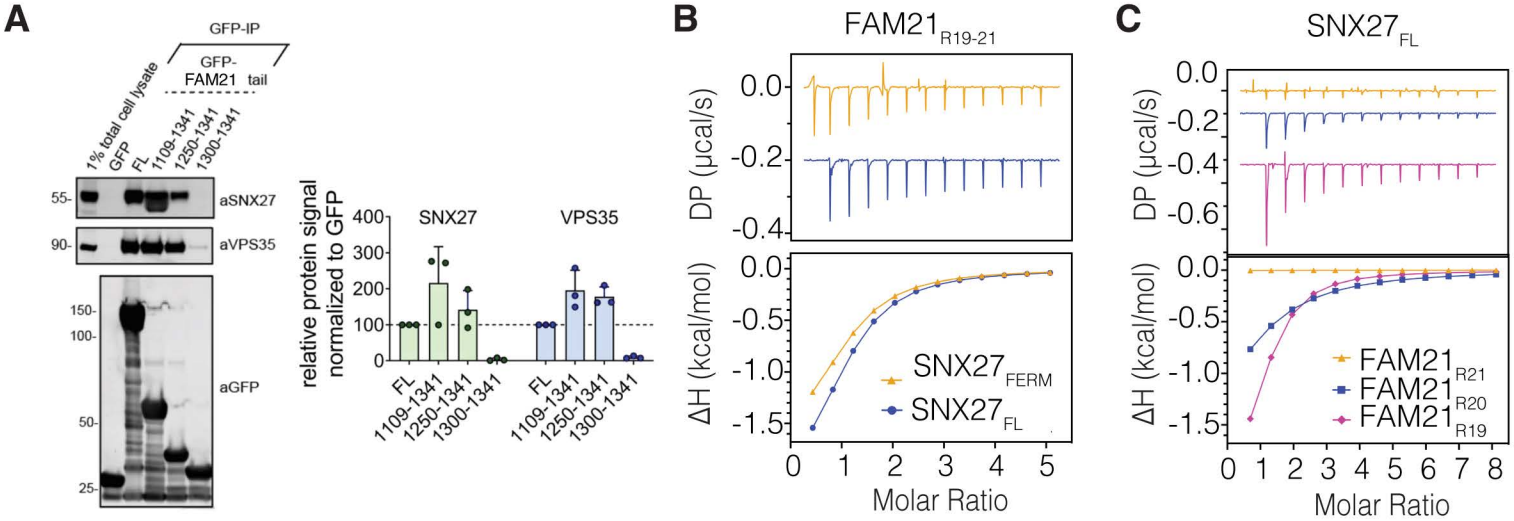

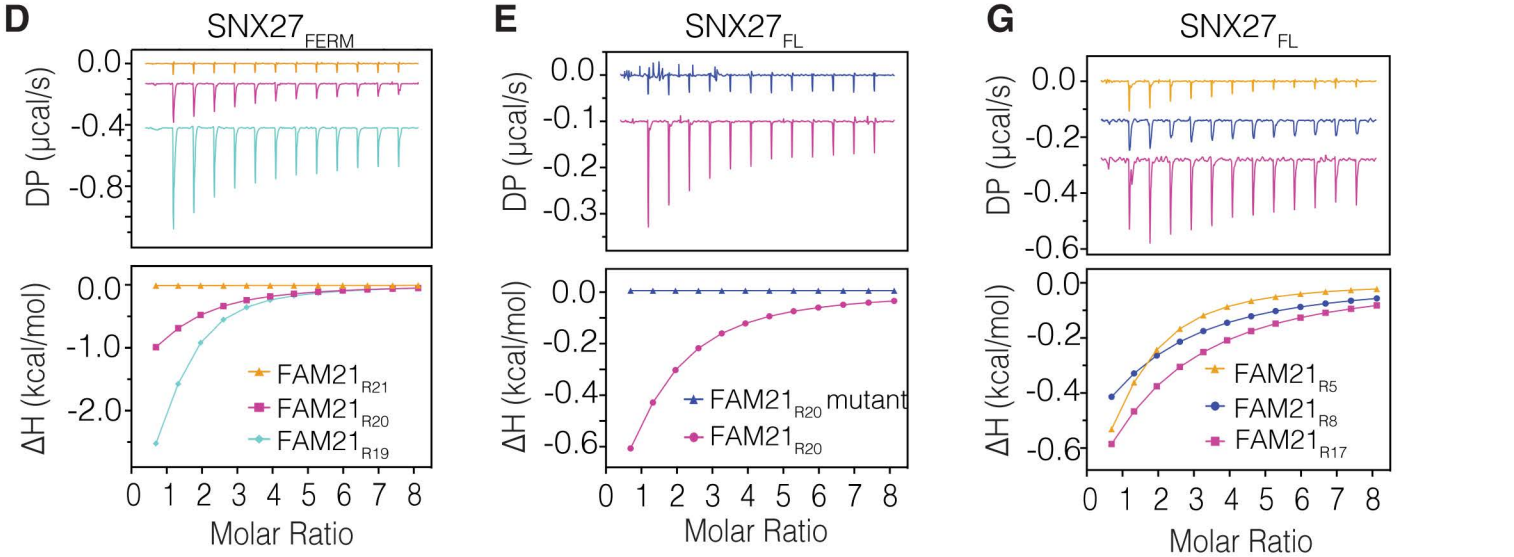

F

FAM21	Range	aDLF sequence	SNX27 (Kd)	SNX27FERM (Kd)
FAM21-R1	367-378	---LFDDEDEESDLF--------	/	/
FAM21-R4	482-491	-----IFGDEEGDLF--------	/	/
FAM21-R5	537-548	---LFSDEEDSEDLF--------	23.55	29.20
FAM21-R8	664-674	----LFEEDKEDDLF--------	68.80	42.50
FAM21-R13	856-862	--------DPDVDLF--------	/	/
FAM21-R14	878-888	----LFGDDEDDDLF--------	/	/
FAM21-R15	1126-1136	----EADLFDSGDIF--------	/	31.70
FAM21-R16	1171-1185	MFPALGEASSDDDLF--------	/	/
FAM21-R17	1201-1209	------LLEDEDDLF--------	70.55	31.79
FAM21-R18	1234-1240	--------IFEDDIF--------	/	/
FAM21-R19	1262-1270	------LFDDNIDIF--------	6.96	38.35
FAM21-R20	1290-1299	-----IFDDDMDDIF--------	19.00	25.55

SNX-BAR	Range	aDLF Sequence
SNX1	35-51	--EAGDSDTEGEDIFTGAA----
SNX1	75-92	NGIHEEQDQEPQDLFADA-----
SNX2	22-35	--------EDGEDLFTSTVSTL-
SNX2	62-82	--TEVVLDDDREDLFAEATEEVS

"/" = no data

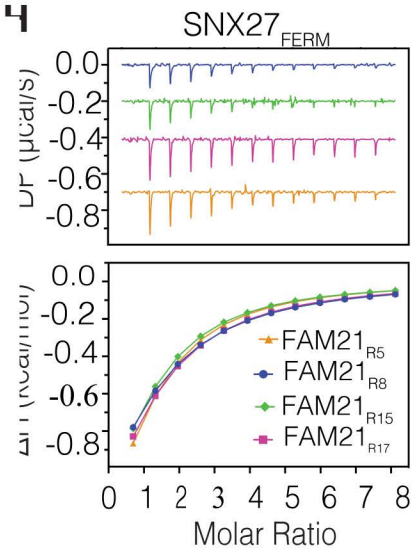

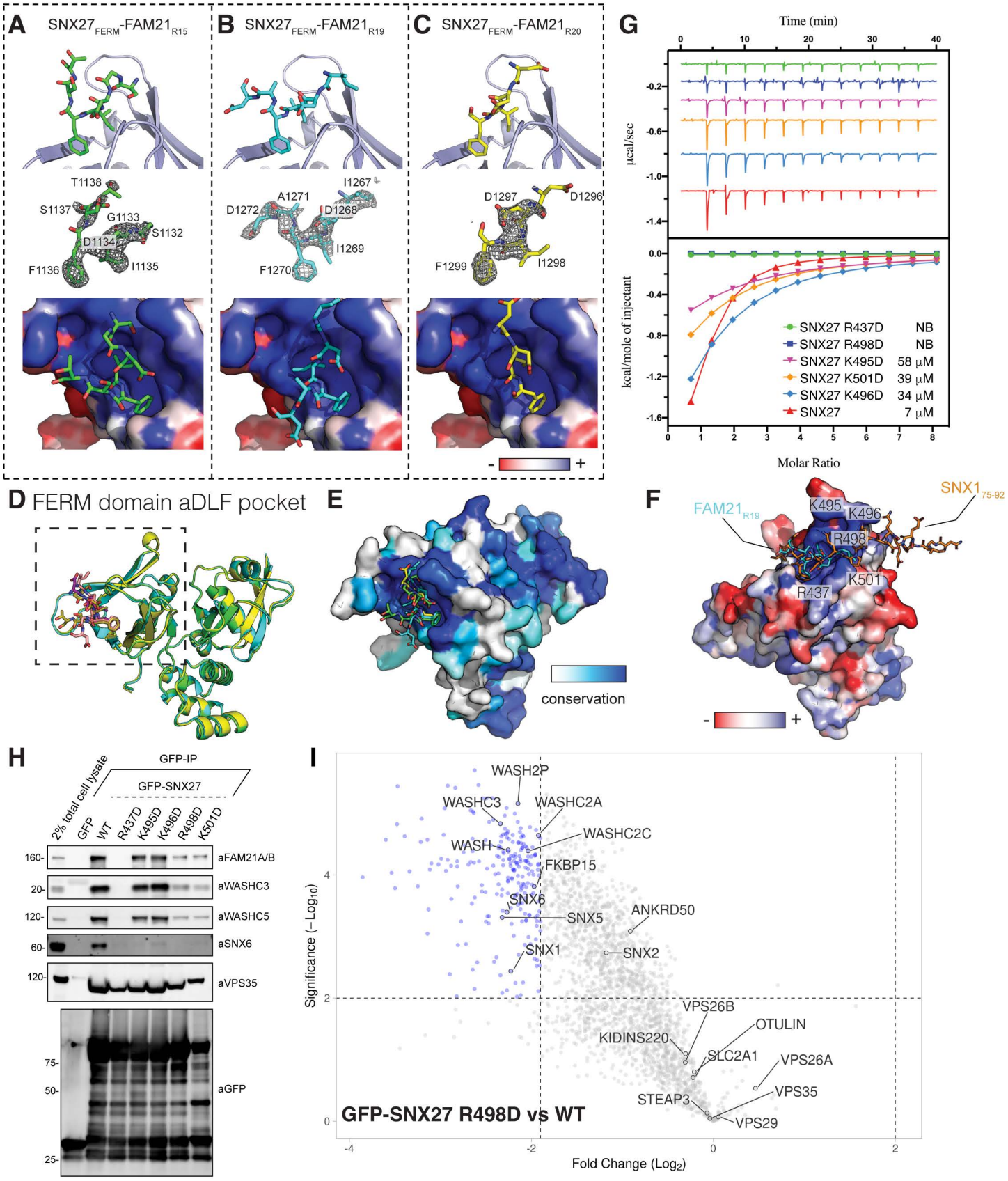
A SNX27FERM-FAM21R15
B SNX27FERM-FAM21R19
C SNX27FERM-FAM21R20
T1138
S1137
G1133
S1132
D1134
F1136
I1135
A1271
I1267
D1272
D1268
I1269
F1270
D1297
D1296
F1299
I1298
-
+
G
Time (min)
µcal/sec
kcal/mole of injectant
SNX27 R437D NB
SNX27 R498D NB
SNX27 K495D 58 µM
SNX27 K501D 39 µM
SNX27 K496D 34 µM
SNX27 7 µM
Molar Ratio
D FERM domain aDLF pocket
E
conservation
F
FAM21R19
SNX175-92
K495
K496
R498
K501
R437
-
+
H
GFP-IP
GFP-SNX27
2% total cell lysate
GFP
WT
R437D
K495D
K496D
R498D
K501D
aFAM21A/B
aWASHC3
aWASHC5
aSNX6
aVPS35
aGFP
I
WASH2P
WASHC3
WASHC2A
WASHC2C
WASH
FKBP15
SNX6
SNX5
ANKRD50
SNX1
SNX2
VPS26B
OTULIN
KIDINS220
SLC2A1
VPS26A
VPS35
STEAP3
VPS29
GFP-SNX27 R498D vs WT
Significance (−Log10)
Fold Change (Log2)

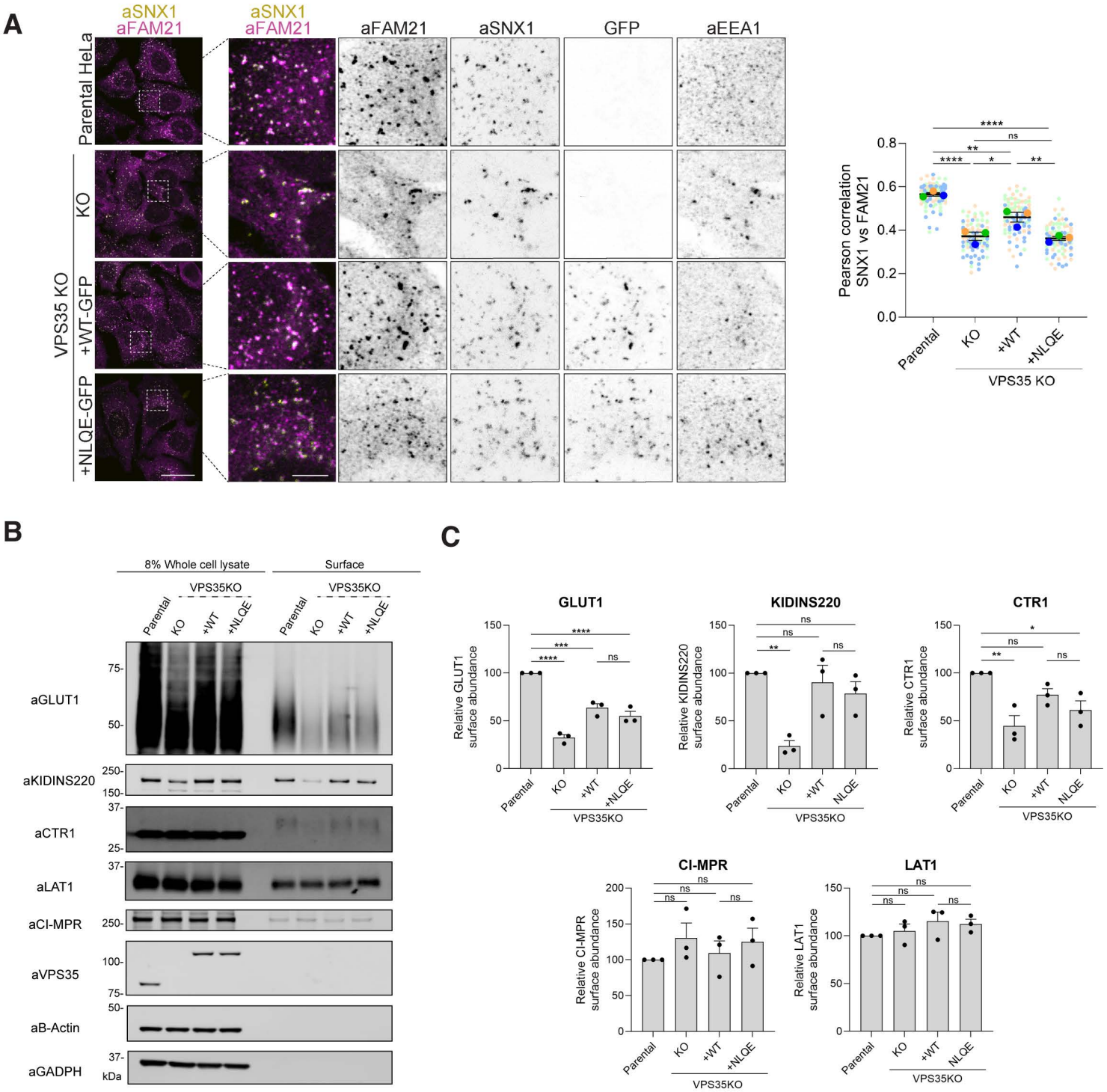
A
aSNX1
aFAM21
aSNX1
aFAM21
aFAM21
aSNX1
GFP
aEEA1
Parental HeLa
VPS35 KO
KO
+WT-GFP
+NLQE-GFP
Pearson correlation SNX1 vs FAM21
Parental
KO
+WT
+NLQE
VPS35 KO
B
8% Whole cell lysate
Surface
VPS35KO
Parental
KO
+WT
+NLQE
aGLUT1
aKIDINS220
aCTR1
aLAT1
aCI-MPR
aVPS35
aB-Actin
aGADPH
kDa
C
GLUT1
KIDINS220
CTR1
CI-MPR
LAT1
Relative GLUT1 surface abundance
Relative KIDINS220 surface abundance
Relative CTR1 surface abundance
Relative CI-MPR surface abundance
Relative LAT1 surface abundance
VPS35KO